www.czasopisma.pan.pl PAN www.journals.pan.pl

Opto-Electronics Review 26 (2018) 236–241

Contents lists available at ScienceDirect

Opto-Electronics Review

journal homepage: http://www.journals.elsevier.com/opto-electronics review

Full Length Article

Ternary photonic crystal with left-handed material layer for refractometric application

S.A. Taya

Physics Department, Islamic University of Gaza, Palestine

ARTICLE INFO

Article history:
Received 31 August 2017
Received in revised form 9 May 2018
Accepted 22 May 2018
Available online 14 July 2018

Keywords:
Photonic crystal
Left-handed material
Sensor
Refractometry application

ABSTRACT

A ternary photonic crystal with left-handed material (LHM) layer is examined for refractometric applications. One of the layers is assumed to be air and treated as an analyte. The transmittance from the ternary photonic crystal is studied in details and the wavelength shift due to the change in the refractive index of the analyte is investigated. The transmittance is investigated with the parameters of the LHM. It is found that the wavelength shift can be significantly enhanced with the decrease of both real part of the LHM permittivity and thickness.

1. Introduction

Many researchers were attracted to photonic crystals in recent years due to possible applications in optoelectronics [1–4]. This multilayer structure led to the construction of photonic band gaps which are sometimes called stop bands. The propagation of waves with definite frequency in these bands is not allowed. The width of this band depends on the incidence angle of light, the indices of refraction of the layers and their thicknesses. If all these parameters are maintained constant, then this one-dimensional photonic crystal structure will possess fixed predetermined forbidden bands of definite frequencies. Electromagnetic waves of frequency lying in these bands will be reflected by the structure.

Photonic crystals can be grouped into categories depending on the number of media in one cell. They can be sorted into binary, ternary, quaternary or so on. This classification is mainly dependent on the number of media in one period. The binary photonic crystal comprises two media in the period, the ternary has three media in a period, the quaternary has four media in a period and so on. These periods are repeated many times to form photonic band gap structures.

Ternary photonic crystal structures have received much more interest because of their excellent performance over the binary photonic crystal structures as sensors for refractometric applications [5], omni-directional reflectors [6–8] and optical filters [9]. The ternary photonic structures may be constructed by the repetition of three materials. The one-dimensional binary photonic crystal can be created by the repetition of two media. The one-dimensional ternary photonic band gap structures exhibit also superior temperature sensing elements [10].

Materials are described by their permittivity ε and permeability μ. Some materials have simultaneous negative electric permittivity and magnetic permeability μ. Those materials have received high interest due to the possibility of being used in many fields. They were referred to as left-handed materials (LHMs) because the electric field **E,** magnetic field **H** and wave vector **K** constitute a left-handed set. LHMs were first studied theoretically by the Russian physicist Veselago in 1968 [11]. They have many properties which are different from normal materials with positive ε and μ. Pendry *et al.* was the first to show the possibility of LHM design by some novel man-made materials [12,13]. Shelby *et al.* fabricated the first LHM in 2001 [14]. Since his wonderful discovery, slab waveguide structures having left-handed material layer have become an interesting topic [15].

Using a slab waveguide as optical sensors is the most recent application of waveguides. They have been utilized as efficient sensors for environmental monitoring, pharmaceutical industry, and food technology. They have many advantages over other sensors such as immunity to light interference [16], fast response, reduced weight and size, resistance to aggressive environments, and easy to interface with optical data communication systems.

One of the advantages of slab waveguides and optical fibers is their immunity to electromagnetic interference. It is well known that all metal cable network media have a common problem since they are at risk of electromagnetic interference. Slab waveguides

E-mail address: staya@iugaza.edu.ps

https://doi.org/10.1016/j.opelre.2018.05.002
1230-3402/

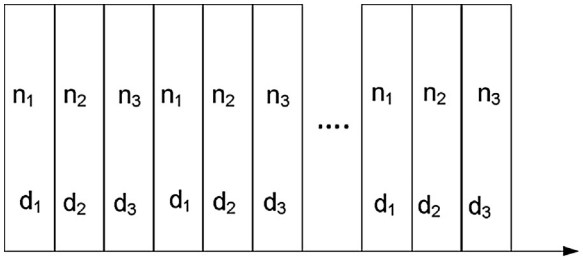

Fig. 1. Ternary photonic crystal with three layers having the indices n_1, n_2 and n_3.

and optical fibers do not suffer from that problem because they are immune to crosstalk since they do not conduct electricity and guide light signals in a dielectric medium rather than electrical signals along a metallic conductor, to transmit data. So they cannot produce a magnetic field result in immune to electromagnetic interference.

In 1989, Tiefenthaler *et al.* studied a slab waveguide for humidity sensing by measuring the change in the effective index of refraction due to any variation in the material contained in the cladding [17]. Since then, considerable research has been conducted to miniature the system and enhance the sensitivity of slab waveguide sensors. Moreover, optical fibers have been used in biosensing in the past few years [18,19]. Surface plasmon resonance (SPR) has been proposed in the field of refractometry [20–22]. Metal-clad waveguide (MCWG) design is one of the most commonly used structures as an optical sensor [23–25]. MCWG structure is the same as a waveguide structure of three layers with an extra metal layer. The metal layer is usually sandwiched between the semi-infinite substrate and the core film. Waveguide sensors are recognized as evanescent field sensors because the evanescent wave is responsible for the sensing operation [26,27]. Any change in the analyte index causes a change in the modal index of the guided mode.

In this work, we report the use of one-dimensional ternary photonic crystal in optical sensing applications. The layers of the ternary photonic crystal are dielectric / LHM / air repeated N times in a periodic structure. The transmission spectrum from the proposed structure is investigated and the wavelength shift due to the change in the refractive index of air is calculated with different parameters of the structure. To the best of my knowledge, this is the first time an LHM is used as a layer in a ternary photonic crystal for optical sensing applications and this is the novel scientific contribution of the current work.

2. Theory

Figure 1 shows a schematic diagram of the proposed photonic crystal. It consists of three layers having the indices n_1, n_2 and n_3 with thicknesses d_1, d_2 and d_3, respectively. The period of the lattice is given by $d = d_1 + d_2 + d_3$. Layer 2 is considered LHM of negative parameters (ε_2, μ_2). The index of refraction n_2 can be calculated as $n_2 = -\sqrt{\varepsilon_2 \mu_2}$.

The characteristic matrix of a cell consisting of three layers is given by

$$\mathrm{M[d]} = \prod_{i=1}^{l} \begin{bmatrix} \cos\beta_i & \frac{-i\sin\beta_i}{p_i} \\ -ip_i\sin\beta_i & \cos\beta_i \end{bmatrix} = \begin{bmatrix} M_{11} & M_{12} \\ M_{21} & M_{22} \end{bmatrix} \quad (1)$$

Where $l = 3$, $\beta 1 = \frac{2\pi n_1 d_1 \cos\theta_1}{\lambda_0}$, $\beta_2 = \frac{2\pi n_2 d_2 \cos\theta_2}{\lambda_0}$, $\beta_3 = \frac{2\pi (n_3) d_3 \cos\theta_3}{\lambda_0}$, $p_1 = \sqrt{\frac{\varepsilon_1}{\mu_1}}\cos\theta_1$, $p_2 = \sqrt{\frac{\varepsilon_2}{\mu_2}}\cos\theta_2$ and $p_3 = \sqrt{\frac{\varepsilon_3}{\mu_3}}\cos\theta_3$. and λ_o is the free space wavelength.

θ_1, θ_2 and θ_3 are the angles which the ray makes with the normal to the interfaces in layers 1, 2 and 3, respectively. They are connected to the incidence angle θ_0 through

$$\cos\theta_1 = \left[1 - \frac{n_0^2 sin^2\theta_0}{n_1^2}\right]^{\frac{1}{2}}, \cos\theta_2 = \left[1 - \frac{n_0^2 sin^2\theta_0}{n_2^2}\right]^{\frac{1}{2}}$$

$$\text{and } \cos\theta_3 = \left[1 - \frac{n_0^2 sin^2\theta_0}{(n_3)^2}\right]^{\frac{1}{2}}.$$

The derivation of matrix M is provided in Appendix A.

Inspection of the determinant of the matrix M[d] in Eq. (1), we find that $\left|M[d]\right| = 1$.

If the system under consideration has N periods, the characteristic matrix is written as

$$[M(d)]^N = \begin{bmatrix} M_{11}T_{N-1}(a) - T_{N-2}(a) & M_{12}T_{N-1}(a) \\ M_{21}T_{N-1}(a) & M_{22}T_{N-1}(a) - T_{N-2}(a) \end{bmatrix} = \begin{bmatrix} m_{11} & m_{12} \\ m_{21} & m_{22} \end{bmatrix} \quad (2)$$

where

$$M_{11} = \left(\cos\beta_1\cos\beta_2\cos\beta_3 - \frac{p_2\sin\beta_1\sin\beta_2\cos\beta_3}{p_1} - \frac{p_3\cos\beta_1\sin\beta_2\sin\beta_3}{p_2} - \frac{p_3\sin\beta_1\cos\beta_2\sin\beta_3}{p_1}\right) \quad (3)$$

$$M_{12} = -i\left(\frac{\sin\beta_1\cos\beta_2\cos\beta_3}{p_1} + \frac{\cos\beta_1\sin\beta_2\cos\beta_3}{p_2} + \frac{\cos\beta_1\cos\beta_2\sin\beta_3}{p_3} - \frac{p_2\sin\beta_1\sin\beta_2\sin\beta_3}{p_1 p_2}\right) \quad (4)$$

$$M_{21} = -i\left(p_1\sin\beta_1\cos\beta_2\cos\beta_3 + p_2\cos\beta_1\sin\beta_2\cos\beta_3 + p_3\cos\beta_1\cos\beta_2\sin\beta_3 - \frac{p_1 p_3\sin\beta_1\sin\beta_2\sin\beta_3}{p_2}\right), \quad (5)$$

$$M_{22} = \left(\cos\beta_1\cos\beta_2\cos\beta_3 - \frac{p_1\sin\beta_1\sin\beta_2\cos\beta_3}{p_2} - \frac{p_2\cos\beta_1\sin\beta_2\sin\beta_3}{p_3} - \frac{p_1\sin\beta_1\cos\beta_2\sin\beta_3}{p_3}\right) \quad (6)$$

T_N are well-known functions called Chebyshev polynomials of the second kind

$$T_N(a) = \frac{\sin\left[(N+1)cos^{-1}a\right]}{\left[1 - a^2\right]^{\frac{1}{2}}}, \quad (7)$$

where

$$a = \frac{1}{2}[M_{11} + M_{22}]. \quad (8)$$

Using the matrix elements m_{ij}, the transmission coefficient of the stack of layers can be written as

$$t = \frac{2p_0}{(m_{11} + m_{12}p_0)p_0 + (m_{21} + m_{22}p_0)}. \quad (9)$$

where

$$p_o = n_0\cos\theta_0 = \cos\theta_0. \quad (10)$$

with $n_0 = 1$.

The transmittance is then given by

$$T = |t|^2. \quad (11)$$

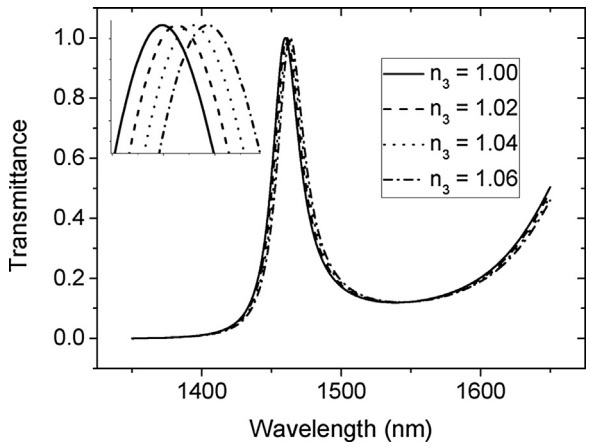

Fig. 2. Transmittance *vs.* wavelength for the ternary photonic crystal with different values of Δn_3 for $N=6$, $n_1=1.54$, $\varepsilon_2=-5.5+0.01i$, $\mu_2=-5.0+0.01i$, $n_2=-\sqrt{(-5.5+0.01i)(-5.0+0.01i)}$, $d_1=100$ nm, $d_2=30$ nm, and $d_3=100$ nm.

3. Results and discussion

A ternary photonic crystal was assumed with the structure dielectric / LHM / air. The following parameters are assumed $N=6$, $n_1=1.54$, $\varepsilon_2=-5.5+0.01i$ [28], $\mu_2=-5.0+0.01i$ [28], $n_2=-\sqrt{(-5.5+0.01i)(-5.0+0.01i)}$, $d_1=100$ nm, $d_2=30$ nm, and $d_3=100$ nm. We first assume normal incidence of $\theta_o=0^\circ$. The transmission spectrum of the one-dimensional ternary photonic crystal is shown in Fig. 2 for $\Delta n_3=0.02$, 0.04, and 0.06. The wavelength was varied from 1350 nm to 1650 nm in steps of 0.1 nm. It was observed that the transmission spectrum of the ternary photonic crystal shows narrow transmission peaks. The peak shifts toward larger wavelengths for any increase in the refractive index of the analyte is clear. This shift in the transmission spectrum is the key in the sensing process. Solid, dashed, dotted and dash dotted curves correspond to $n_3=1.00$, 1.02, 1.04 and 1.06. The solid curve transmission peak has a central wavelength at 1459.9 nm for $\Delta n_3=0.00$. The dashed curve transmission peak has a central wavelength at 1461 nm whereas the dotted curve is centered at 1462.2 for $\Delta n_3=0.02$ and 0.04, respectively. The dashed dotted curve has its center at a wavelength of 1463.4 for $\Delta n_3=0.06$. The sensitivity of the proposed sensor can be evaluated as $\Delta\lambda/\Delta n$ which is given by 58.3 nm. This is a high shift and can be detected easily with existing optoelectronic devices.

We now try to optimize ε_2 and d_2 of the LHM to find out the values corresponding to the maximum shift in the transmission peak. Figure 3 shows the transmission spectrum of the one-dimensional ternary photonic crystal for $\varepsilon_2=-6.0+0.01i$, $-5.5+0.01i$, $-5.0+0.01i$ and $-4.5+0.01i$. The transmission spectrum of the ternary photonic crystal shows transmission peak shifts for any increase in the refractive index of the analyte. Solid, dashed, dotted and dash dotted curves correspond to $n_3=1.00$, 1.02, 1.04 and 1.06. For $\varepsilon_2=-6.0+0.01i$ (upper left panel), the sensitivity of the photonic crystal sensor is found to be $\Delta\lambda/\Delta n=56.67$ nm. When ε_2 is decreased to $\varepsilon_2=-5.5+0.01i$ (upper right panel), the sensitivity is found to be $\Delta\lambda/\Delta n=58.3$ nm. If ε_2 is decreased again to $\varepsilon_2=-5.0+0.01i$ (lower left panel), the sensitivity is $\Delta\lambda/\Delta n=61.67$ nm. Finally if ε_2 is decreased to become $\varepsilon_2=-4.5+0.01i$, we find that $\Delta\lambda/\Delta n=105$ nm. As can be seen from Fig. 3, the wavelength shift can be considerably enhanced with the decrease of the absolute value of the real part of the LHM permittivity.

The transmission spectrum of the one-dimensional ternary photonic crystal is plotted in Fig. 4 for $d_2=24$ nm, 26 nm, 28 nm and 30 nm. The transmission peaks shift for any increase in the refractive index of the analyte can be seen clearly in the figure. For $d_2=24$ nm, the solid curve transmission peak has a central wavelength at 1534.6 nm for $\Delta n_3=0.00$ whereas the dashed curve transmission peak has a central wavelength at 1536.6 nm for $\Delta n_3=0.02$. The dotted curve is centered at 1538.7 for $\Delta n_3=0.04$ and the dashed dotted curve has its center at a wavelength of 1540.9 for $\Delta n_3=0.06$. As seen, the transmission peak exhibits a wavelength shift of 6.3 nm for $\Delta n_3=0.06$ revealing a sensitivity of $\Delta\lambda/\Delta n=105$ nm. On the other hand it shows a sensitivity of $\Delta\lambda/\Delta n=101$ nm, 61.67 nm, and 58.33 for $d_2=26$ nm, 28 nm and 30 nm, respectively. As observed from Fig. 4, the wavelength shift can be significantly improved with the decrease of the LHM thickness.

If we move to the oblique incidence and examine the wavelength shift with the angle of incidence as illustrated in Fig. 5. As

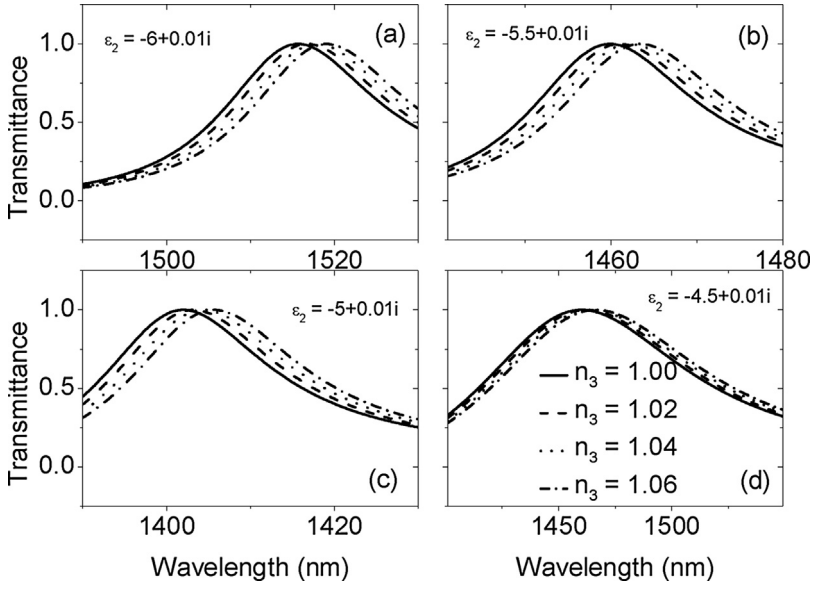

Fig. 3. Transmittance *vs.* wavelength for the ternary photonic crystal with different values of Δn_3 for different values of ε_2, $N=6$, $n_1=1.54$, $\mu_2=-5.0+0.01i$, $n_2=-\sqrt{\varepsilon_2(-5.0+0.01i)}$, $d_1=100$ nm, $d_2=30$ nm, and $d_3=100$ nm.

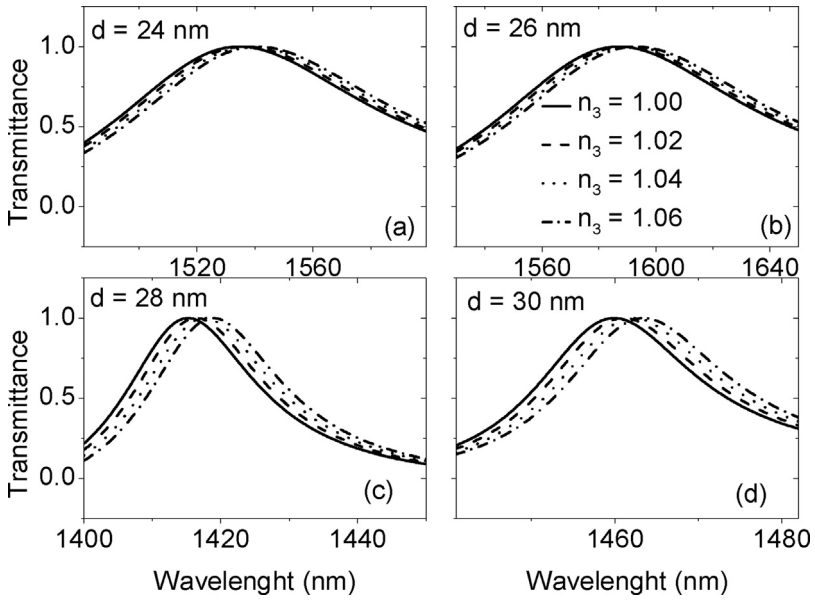

Fig. 4. Transmittance *vs.* wavelength for the ternary photonic crystal with different values of Δn_3 for different values of d_2, $N = 6$, $n_1 = 1.54$, $\varepsilon_2 = -5.5 + 0.01i$, $\mu_2 = -5.0 + 0.01i$, $n_2 = -\sqrt{(-5.5 + 0.01i)(-5.0 + 0.01i)}$, $d_1 = 100$ nm, and $d_3 = 100$ nm.

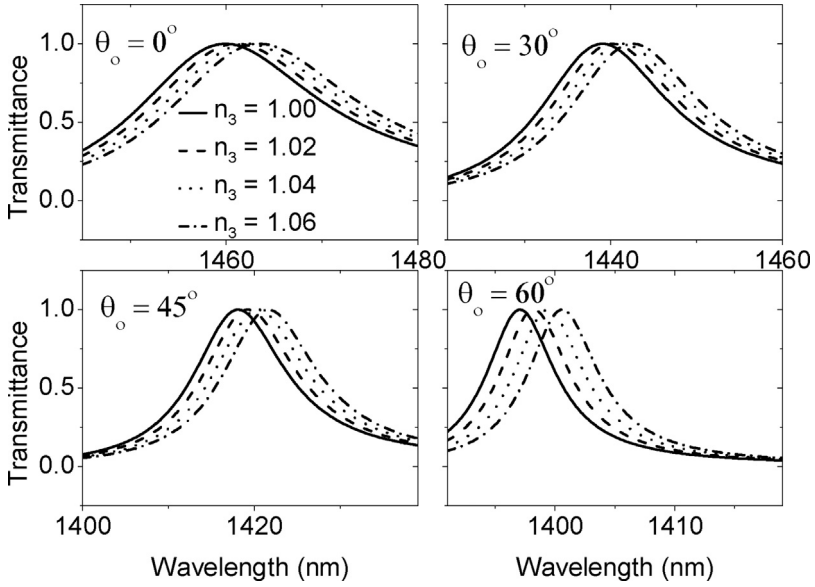

Fig. 5. Transmittance *vs.* wavelength for the ternary photonic crystal with different values of Δn_3 for different values of the incidence angle, $N = 6$, $n_1 = 1.54$, $\varepsilon_2 = -5.5 + 0.01i$, $\mu_2 = -5.0 + 0.01i$, $n_2 = -\sqrt{(-5.5 + 0.01i)(-5.0 + 0.01i)}$, $d_1 = 100$ nm, and $d_3 = 100$ nm.

can be seen from the figure, the incidence angle has no effect of the wavelength shift. For $\theta_o = 0^\circ$, 30°, 45° and 60°, the wavelength shift reaches 3.5 nm for all angles of incidence for $n_3 = 1.06$ compared to $n_3 = 1.00$ and the sensitivity is estimated as $\Delta\lambda/\Delta n = 58.33$ nm.

It is worth comparing the results of the current work with the state of the art sensitivity. In a recent work [5], a ternary photonic crystal was proposed as a refractometric sensor for detection small changes in the index of refraction of an analyte. The obtained sensitivity in their work was $\Delta\lambda/\Delta n = 350$ nm whereas we could achieve a sensitivity of about $\Delta\lambda/\Delta n = 105$ nm for some configuration of the proposed photonic crystal. However, the obtained sensitivity can be adjusted and considerably increased by choosing the appropriate parameters of the LHM.

4. Conclusions

One-dimensional ternary photonic crystal with left-handed material layer is examined for refractometric applications. One of the layers is assumed to be air and treated as an analyte. The transmission spectrum from the one-dimensional ternary photonic crystal is studied in details and the wavelength shift due to the change in the index of an analyte is investigated with different parameters of the structure. It was observed that the transmission peak shows a shift of 0.583 nm for each refractive index change of 0.01. This shift is high enough to be detected easily with existing optoelectronic devices. The sensitivity of the proposed sensor was evaluated as $\Delta\lambda/\Delta n$ and found 58.3 nm. We studied the

sensitivity with the permittivity of the LHM and found that for $\varepsilon_2 = -6.0 + 0.01i$, $\varepsilon_2 = -5.5 + 0.01i$, $\varepsilon_2 = -5.0 + 0.01i$ and $\varepsilon_2 = -4.5 + 0.01i$ the proposed photonic crystal has the sensitivities $\Delta\lambda/\Delta n$ = 56.67 nm, 58.3 nm, 61.67 nm and 105 nm, respectively. Moreover, we investigated the wavelength shift with the LHM thickness and observed that for d_2 = 24 nm, 26 nm, 28 nm and 30 nm the structure exhibited sensitivities of $\Delta\lambda/\Delta n$ = 105 nm, 101 nm, 61.67 nm and 58.33, respectively.

The wavelength shift can be significantly improved with the decrease of the LHM thickness and the LHM permittivity. We also found that the incidence angle has no effect of the wavelength shift.

Appendix A.

Let the plane of incidence be y–z plane, then for TE mode, $E_y = E_z = 0$. The solution of the wave equation can be written as [29]

$$E_x = U(z)e^{i(k_0 by-\omega t)} \tag{A.1}$$

$$H_y = V(z)e^{i(k_0 by-\omega t)} \tag{A.2}$$

$$H_z = W(z)e^{i(k_0 by-\omega t)} \tag{A.3}$$

where k_0 is the wavenumber in the vacuum, ω is the wave frequency and $b = n\sin\theta$, where θ denotes the angle which the ray makes with the normal and n is the index of refraction. After substitutions in Maxwell's equation, U, V and W are related to each other by the following equations

$$\acute{U} = ik_0\mu V \tag{A.4}$$

$$\acute{V} = ik_0(\varepsilon - \frac{b^2}{\mu})U \tag{A.5}$$

$$bU + \mu W = 0 \tag{A.6}$$

U, V can be expressed as combinations of two particular solutions as

$$\acute{U}_1 = ik_0\mu V_1 \tag{A.7}$$

$$\acute{U}_2 = ik_0\mu V_2, \tag{A.8}$$

$$\acute{V}_1 = ik_0(\varepsilon - \frac{b^2}{\mu})U_1 \tag{A.9}$$

$$\acute{V}_2 = ik_0\left(\varepsilon - \frac{b^2}{\mu}\right)U_2. \tag{A.10}$$

The relations (7–10) follow that

$$U_1\acute{V}_2 - \acute{V}_1U_2 = 0 \tag{A.11}$$

$$V_1\acute{U}_2 - \acute{U}_1V_2 = 0 \tag{A.12}$$

$$\frac{d}{dZ}(U_1V_2 - U_2V_1) = 0 \tag{A.13}$$

For our purpose, the most convenient choice of the particular solution is

$$U_1 = f(z),\ U_2 = F(z),\ V_1 = g(z),\ V_2 = G(z) \tag{A.14}$$

such that

$$f(0) = G(0) = 0 \text{ and } F(0) = g(0) = 1. \tag{A.15}$$

The solutions with $U(0) = U_0$, $V(0) = V_0$ may be expressed in the form

$$U = FU_0 + fV_0, \tag{A.16}$$

$$V = GU_0 + gV_0. \tag{A.17}$$

or in matrix notation

$$Q = NQ_0 \tag{A.18}$$

where

$$Q = \begin{bmatrix} U(z) \\ V(z) \end{bmatrix},\ Q_0 = \begin{bmatrix} U_0 \\ V_0 \end{bmatrix},\ N = \begin{bmatrix} F(z) & f(z) \\ G(z) & g(z) \end{bmatrix}, \tag{A.19}$$

then

$$Q_0 = MQ \tag{A.20}$$

where

$$M = \begin{bmatrix} g(z) & -f(z) \\ -G(z) & F(z) \end{bmatrix}. \tag{A.21}$$

Now differentiating Eq. (A.4) with respect to z and substituting from Eq. (A.5), we get

$$\frac{d^2U}{dz^2} + {k_0}^2\left(n^2 - b^2\right)U = 0. \tag{A.22}$$

Differentiating Eq. (A.5) with respect to z and substituting from Eq. (A.4), we get

$$\frac{d^2V}{dz^2} + {k_0}^2\left(n^2 - b^2\right)V = 0. \tag{A.23}$$

Substituting for $b = n\sin\theta$

$$\frac{d^2U}{dz^2} + ({k_0}^2n^2\cos^2\theta)U = 0. \tag{A.24}$$

$$\frac{d^2V}{dz^2} + +({k_0}^2n^2\cos^2\theta)V = 0. \tag{A.25}$$

The solution of the above equations is given by

$$U(z) = A\cos(k_0nz\cos\theta) + B\sin(k_0nz\cos\theta) \tag{A.26}$$

$$V(z) = \frac{1}{i}\sqrt{\frac{\varepsilon}{\mu}}\cos\theta\left[B\cos\left(k_onz\cos\theta\right) - A\sin(k_0nz\cos\theta)\right]. \tag{A.27}$$

Applying the boundary condition in Eq. (A.15) and making use of Eq. (A.14), we get

$$U_1 = f(z) = \frac{i}{\cos\theta}\sqrt{\frac{\mu}{\varepsilon}}\sin(k_0nz\cos\theta) \tag{A.28}$$

$$U_2 = F(z) = \cos\left(k_0nz\cos\theta\right), \tag{A.29}$$

$$V_1 = g(z) = \cos(k_0nz\cos\theta) \tag{A.30}$$

$$V_2 = G(z) = i\sqrt{\frac{\varepsilon}{\mu}}\sin(k_0nz\cos\theta) \tag{A.31}$$

$$\begin{pmatrix} U_0 \\ V_0 \end{pmatrix} = \begin{pmatrix} \cos(k_0nz\cos\theta) & -\frac{i}{p}\sin(k_0nz\cos\theta) \\ -ip\sin(k_0nz\cos\theta) & \cos(k_onz\cos\theta) \end{pmatrix}\begin{pmatrix} U \\ V \end{pmatrix}. \tag{A.32}$$

References

[1] S. Sandhu, S. Fan, M. Yanik, M. Povinelli, Advances in theory of photonic crystal, J. Light Wave Technol. 24 (2006) 4493–4501.
[2] I. Kriegel, F. Scotognella, Disordered one-dimensional photonic structures composed by more than two materials with the same optical thickness, Opt. Commun. 338 (2015) 523–527.
[3] Z. Zare, A. Gharaati, Investigation of band gap width in ternary 1D photonic crystal with left-handed laye, Acta Phys. Pol. A 125 (2014) 36–38.
[4] C.J. Wu, Y.H. Chung, T.J. Yang, B.J. Syu, Band gap extension in a one-dimensional ternary metal-dielectric photonic crystal, Prog. Electromagn. Res. 102 (2010) 81–93.
[5] A. Banerjee, Enhanced refractometric optical sensing by using one-dimensional ternary photonic crystals, Prog. Electromagn. Res., PIER 89 (2009) 11–22.
[6] S.K. Awasthi, U. Malaviya, S.P. Ojha, Enhancement of omnidirectional total-reflection wavelength range by using one dimensional ternary photonic band gap material, J. Opt. Soc. Am. B 23 (2006) 2566–2571.
[7] F. Xue, S. Liu, H. Zhang, X. Kong, Y. Wen, Wang L, S. Qian, The theoretical analysis of omnidirectional photonic band gaps in the one-dimensional

ternary plasma photonic crystals based on Pell quasi-periodic structure, Opt. Quant. Electron. 49 (2017) 19.
[8] S. Sharma, R. Kumar, K. Singh, A. Kumar, V. Kumar, Omnidirectional reflector using linearly graded refractive index profile of 1D binary and ternary photonic crystal, Optik 126 (2015) 1146–1149.
[9] S.K. Awasthi, S.P. Ojha, Design of a tunable optical filter by using one-dimensional ternary photonic band gap material, Prog. Electromagn. Res. M 4 (2008) 117–132.
[10] A. Banerjee, Enhanced temperature sensing by using one-dimensional ternary photonic band gap structures, Prog. Electromagn. Res. Lett. 11 (2009) 129–137.
[11] V.G. Veselago, The electrodynamics of substances with simultaneously negative values of ε and μ, Sov. Phy. Usp. 10 (1968) 509–514.
[12] J.B. Pendry, A.J. Holden, W.J. Stewart, I. Youngs, Extremely low frequency plasmons in mettalic mesostructures, Phys. Rev. Lett. 76 (1996) 4773–4776.
[13] J.B. Pendry, A.J. Holden, D.J. Robbins, W.J. Stewart, Magnetism from conductors and enhanced nonlinear phenomena, IEEE. Trans. Microw. Theory Tech. 47 (1999) 2075–2090.
[14] R.A. Shelby, D.R. Smith, S. Schultz, Experimental verification of a negative index of refraction, Science 292 (2001) 77–79.
[15] S.A. Taya, Dispersion properties of lossy, dispersive, and anisotropic left-handed material slab waveguide, Optik 126 (2015) 1319–1323.
[16] S.A. Taya, Theoretical investigation of slab waveguide sensor using anisotropic metamaterials, Opt. Appl. 45 (2015) 405–417.
[17] K. Tiefenthaler, W. Lukosz, Sensitivity of grating couplers as integrated-optical chemical sensors, J. Opt. Soc. Am. B 6 (1989) 209–220.
[18] R. Horvath, G. Fricsovszky, E. Pap, Application of the optical waveguide light mode spectroscopy to monitor lipid bilayer phase transition, Biosens. Bioelectron. 18 (2003) 415–428.
[19] B. Kuswandi, Simple optical fiber biosensor based on immobilized enzyme for monitoring of trace having metal ions, Anal. Bioanal. Chem. 376 (2003) 1104–1110.
[20] E. Udd, An overview of fiber optic sensors, Rev. Sci. Instrum. 66 (1995) 4015–4030.
[21] F.C. Chien, S.J. Chen, A sensitivity comparison of optical biosensors based on four different surface plasmon resonance modes, Biosens. Bioelectron. 20 (2004) 633–642.
[22] J. Homola, S.S. Yee, G. Gauglitz, Surface plasmon resonance sensors: review, Sens. Actuators B 54 (1999) 3–15.
[23] N. Skivesen, R. Horvath, H. Pedersen, Optimization of metal-clad waveguide sensors, Sens. Actuators B 106 (2005) 668–676.
[24] N. Skivesen, R. Horvath, H. Pedersen, Peak-type and dip-type metal-clad waveguide sensing, Opt. Lett. 30 (2005) 1659–1661.
[25] N. Skivensen, R. Horvath, S. Thinggaaed, N.B. Larsen, H.C. Pedersen, Deep-probe metal-clad waveguide biosensors, Biosens. Bioelectron. 22 (2007) 1282–1288.
[26] S.A. Taya, Slab waveguide with air core layer and anisotropic left-handed material claddings as a sensor, Opto-Electron. Rev. 22 (2014) 252–257.
[27] S.A. Taya, P-polarized surface waves in a slab waveguide with left-handed material for sensing applications, J. Magn. Magn. Mater. 377 (2015) 281–285.
[28] G. Wu, Song Liu, S. Zhong, Numerical analysis of propagation characteristics of electromagnetic wave in lossy left-handed material media, Optik 125 (2014) 4233–4237.
[29] M. Born, E. Wolf, Principles of Optics, Cambridge University Press, United Kingdom, 2003.